ChemCatChem

Research Article
doi.org/10.1002/cctc.202500462

Chemistry Europe
European Chemical Societies Publishing

www.chemcatchem.org

From Hydroborations Catalyzed by Sn(II) Cations to Photoluminescent Boronic Esters

Ondřej Moždiak,[a] Tomáš Bíza,[a] Lukáš Střižík,[a] Zdeňka Růžičková,[a] Milan Erben,[a] Libor Dostál,[a] Emanuel Hupf,[b] and Roman Jambor*[a]

The *N*-coordinated Sn(II) cations [{(2,6-*i*Pr$_2$-C$_6$H$_3$)-N = C(Me)-(6-MeO)-C$_5$H$_3$N}SnCl](SnCl$_3$) (**1**), [{(2,6-*i*Pr$_2$-C$_6$H$_3$)-N = C(Me)-(6-P(O)(O*i*Pr)$_2$)-C$_5$H$_3$N}SnCl](SnCl$_3$) (**2**), and [{(1,2-(C$_5$H$_4$N-2-CH = N)$_2$CH$_2$CH$_2$)}SnCl](SnCl$_3$) (**3**) were prepared and used as catalysts in the hydroboration of ketones and aldehydes. Mechanistic and kinetic studies provide evidence that these electrophiles interact with the C=O bond of the substrates and indicate a pseudo-first-order reaction with a rate constant of k = 70.2 h^{-1} using 2 mol% of **1. 1** could effectively be used as a catalyst in the hydroboration of a broad range of substrates including, substituted benzaldehydes, heterocyclic carbaldehydes, and aliphatic aldehydes, as well as ketones. Finally, **1** was used in large-scale hydroboration reactions of pyridine-substituted carbaldehydes to prepare the respective pyridine-substituted boronic esters [2-(PinBOCH$_2$)-C$_5$H$_4$N] (**4**), [2-(PinBOCH$_2$)-4-(MeO)-C$_5$H$_3$N] (**5**), [2-(PinBOCH$_2$)-6-(MeO)-C$_5$H$_3$N] (**6**), [2-(PinBOCH$_2$)-6-Br-C$_5$H$_3$N] (**7**), [2-(PinBOCH$_2$)-5-Br-C$_5$H$_3$N] (**8**), [3-(PinBOCH$_2$)-C$_5$H$_4$N] (**9**), and borinate [2-[(BBN)OCH$_2$]-4-(MeO)-C$_5$H$_3$N] (**10**), which were characterized by NMR spectroscopy, single-crystal X-ray structure analysis, and an analysis of their photoluminescence.

1. Introduction

Catalytic hydroboration of carbonyl compounds is an efficient method for the preparation of functionalized boron esters or functionalized alcohols.[1] The pinacolborane (HBPin), catecholborane (HBCat), or 9-borabicyklo(3.3.1)nonane (9-BBN) are currently used as mild hydroboration reagents for the selective reduction of the carbonyl group. Due to the lower reactivity of these hydroboration reagents, the presence of a suitable catalyst is required. While transition metal complexes are known as efficient catalysts,[2] those based on main group elements are less explored.[3] Recent advances suggest that group 14 elements, especially Sn(II) compounds, could play a prominent role in the catalytic hydroboration.[3b] Jones´s catalyst based on the sterically protected Sn(II) hydride (Figure 1a) was one of the first hydroboration catalysts of the 14 group elements.[4] Later on, non-hydridic neutral Sn(II) (Figure 1b–g)[5] or ionic Sn(II) compounds (Figure 1h–i) have also been successfully applied for aldehyde hydroborations.[6] Most recently, tin *ansa*-metallocene has also been found to be a potential hydroboration catalyst (Figure 1j).[7]

Mechanistic studies revealed that the catalyzed hydroboration mechanism strongly depends on the type of Sn(II) source. Most of these catalytic hydroboration reactions involve the interaction of the HBPin with the Sn(II) catalyst to form the corresponding Sn*H* bond as an active species. This process is followed by hydrostannylation of the carbonyl R$_2$CO and the generation of the SnO-*CH*R$_2$ moiety, followed by the regeneration of the Sn*H* moiety along with the release of the corresponding boron ester (PinB)O*CH*R$_2$.[4,5c–f]

In a second proposed mechanism, the activation of carbonyl R$_2$CO was suggested to be stemming from the coordination to the Sn(II) serving as an electrophilic center.[2,3] The activated carbonyl group can then be easily reduced by HBpin to form the corresponding boron ester (PinB)O*CH*R$_2$ along with the release of the Sn(II) electrophilic center, re-entering the catalytic cycle and interacting with another carbonyl R$_2$CO.

Recently, our group reported the *N*-coordinated Sn(II) cations [{(2,6-*i*Pr$_2$-C$_6$H$_3$)-N = C(Me)-(6-MeO)-C$_5$H$_3$N}SnCl](SnCl$_3$) (**1**), [{(2,6-*i*Pr$_2$-C$_6$H$_3$)-N = C(Me)-(6-P(O)(O*i*Pr)$_2$)-C$_5$H$_3$N}SnCl](SnCl$_3$) (**2**), and [{(1,2-(C$_5$H$_4$N-2-CH = N)$_2$CH$_2$CH$_2$)}SnCl](SnCl$_3$) (**3**) (Figure 2), which were able to activate the C=O bond of L-lactide and control the ring opening polymerization through the so-called "activated monomer" due to an efficient C=O←Sn(II) interaction.[8a] Therefore, we now set out to test these electrophiles **1**–**3** as potential catalysts in carbonyl hydroboration reactions. For the most efficient complex, mechanistic studies were conducted, and the substrate scope was investigated. In certain cases, the obtained substrates revealed blue-green photoluminescence (PL), and thus large-scale hydroborations were carried out. Finally, these substrates were characterized using NMR spectroscopy and X-

[a] O. Moždiak, T. Bíza, L. Střižík, Z. Růžičková, M. Erben, L. Dostál, R. Jambor
Department of General and Inorganic Chemistry, Faculty of Chemistry and Technology, University of Pardubice, Pardubice 53210, Czech Republic
E-mail: roman.jambor@upce.cz

[b] E. Hupf
Institute of Inorganic Chemistry and Crystallography, University of Bremen 28359, Bremen, Germany

Supporting information for this article is available on the WWW under https://doi.org/10.1002/cctc.202500462

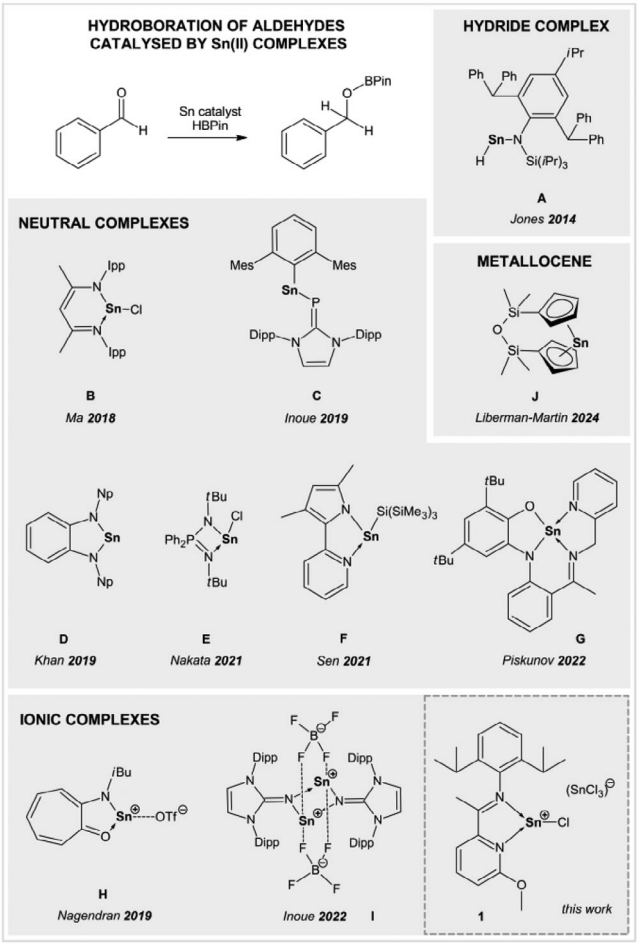

Figure 1. Different Sn(II)-based catalysts used in the hydroboration of aldehydes.

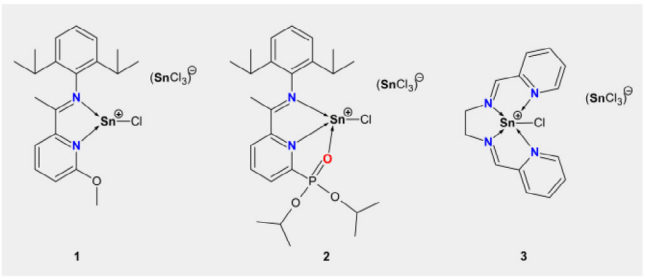

Figure 2. *N,N*-coordinated ionic Sn(II) complexes tested as catalysts for carbonyl hydroboration.

ray structure analysis, and their luminescent properties were also studied.

2. Results and Discussion

2.1. Hydroboration Reactions Catalyzed by 1–3

The ionic Sn-complexes **1–3** (Figure 2) containing *N,N*-coordinated Sn(II) cations were prepared and characterized according to the literature.[8]

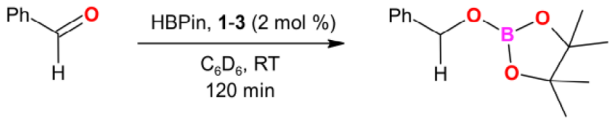

Scheme 1. Hydroboration of benzaldehyde catalyzed by **1–3** (2 mol%), 120 min, RT, C_6D_6.

Table 1. Conversions of the benzaldehyde hydroboration catalyzed by **1–3** (2–0.01 mol%), 120 to 5 min, RT, C_6D_6.

Entry	Cat.	Molar Loading (%)	Time (min)	Conversion (%)[a]	TOF (h^{-1})[b]
1	**1**	2	120	>95	25
2	**2**	2	120	>95	25
3	**3**	2	120	90	23
4	**1**	1	120	>95	50
5	**2**	1	120	70	35
6	**1**	0.25	30	>95	800
7	**1**	0.1	30	>95	1880
8	**1**	0.05	30	>95	4000
9	**1**	0.01	30	94	20,000
10	**1**	2	15	>95	195
11	**1**	0.5	15	>95	800
12	**1**	0.01	15	88	35,600
13	**1**	0.01	5	84	100,800

[a] Conversions detected by ^{1}H NMR of the reaction mixture in C_6D_6.
[b] TOF was calculated: (moles of product/moles of catalyst)/time (h).

However, all complexes **1–3** deviate mutually, with a k^2-*N,N*-three coordinated (**1**), k^3-*N,N,O*-four coordinated (**2**), and finally a k^4-*N,N,N,N*-five coordinated (**3**) Sn(II) center. Therefore, complexes **1–3** were tested as catalysts of aldehyde hydroboration reactions to assess the influence of the Sn coordination arrangement on the catalytic activity. Benzaldehyde (PhCHO) was chosen as a model substrate, and HBPin was used as the hydroboration source (Scheme 1). A mixture of PhCHO (0.5 mmol) with complexes **1–3** (0.01 mmol; 2 mol%) was dissolved in 2 mL of C_6D_6 in a Schlenk tube under inert conditions, and 1 eq. of HBPin (0.5 mmol) was added at once via a syringe.

The mixture was stirred at RT for 2 h, and the conversion was monitored by ^{1}H NMR spectroscopy. All complexes tested in this model reaction were found to be active catalysts (Table 1).

While complexes **1** and **2** showed similar catalytic activity (conversions up to 95%), the κ^4-*N,N,N,N*-five-coordinated Sn(II) cation **3** revealed lower conversion (entry 3, Figures S1–S3). Decreasing the catalytic loading of **1** and **2** to 1 mol% revealed nearly quantitative conversion for **1** (up to 95%, entry 4), while **2** showed lower activity (70%, entry 5; see Figures S4 and S5). Reducing the catalyst loading from **1** to 0.25, 0.1, 0.05, and 0.01 mol%, respectively, along with decreasing the reaction time from 120 to 5 min, demonstrated the high catalytic activity of **1**, with TOFs exceeding 100,800 h^{-1} (see Figures S6–S13). These experiments showcase that the k^2-*N,N*-three-coordinated Sn(II) cation **1** is the most efficient catalyst in this study and is able to fully

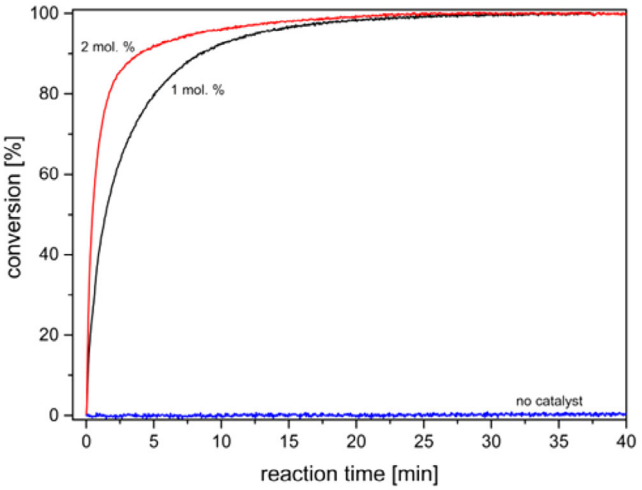

Figure 3. Conversion of benzaldehyde during the hydroboration using Sn-species **1** as a catalyst.

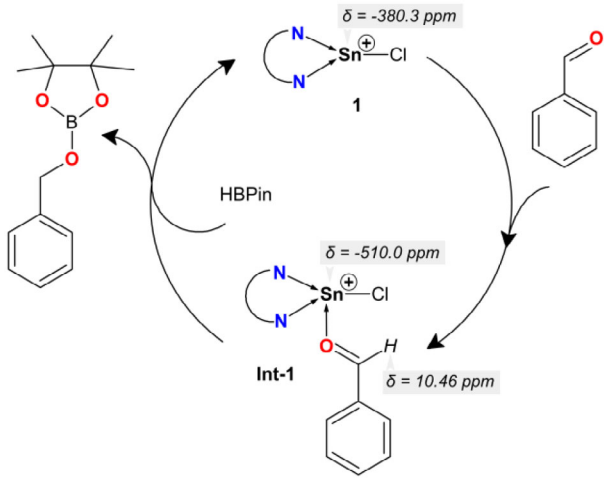

Scheme 2. Proposed mechanism of benzaldehyde hydroboration catalyzed by **1** as suggested by NMR experiments.

reduce benzaldehyde within 15 min with a catalyst loading of 0.5 mol% or within 30 min with a loading of 0.05 mol% (see entries 8 and 11). Additionally, we have then performed additional mechanistic and kinetic studies to gain further insight into this process (for an NMR-based kinetic study of catalyst **2**, see Figures S14–S16). As the reduction of benzaldehyde using catalyst **1** was too fast to be studied effectively on an NMR time scale (see entry 13 in Table 1), we have examined the mechanism of this reaction by time-resolved FTIR spectroscopy in the 2600–800 cm^{-1} region, where chemically significant and assignable vibrations occur. Analysis of the recorded IR spectra revealed the characteristic bands[9a] corresponding to the starting HBPin (ν_{BH} and δ_{BH} at 2580 and 1341 cm^{-1}, respectively) and PhCHO ($\nu_{C=O}$ at 1705 cm^{-1}), along with vibrations of the final dioxaborolane ($\nu_{BO} + \delta_{OBO}$ at 967 cm^{-1}), as shown in Figures S17–S19. These experiments clearly showed that in the absence of the catalyst, no reaction occurs between PhCHO and HBPin (Figure 3). Instead, slow hydrolysis of HBPin was observed (Figure S17). The time-dependent concentration changes of PhCHO and HBPin were nearly identical (Figures S18 and S19), and therefore the catalyzed hydroboration exhibits first-order dependence for both PhCHO and HBPin.[9] Using a literature-reported method,[9] we determined rate constants of 31.8 and 70.2 h^{-1} for a catalyst loading of 1 and 2 mol% of **1**, respectively (see Figures S20 and S21; for comparison rate constants of 0.42 and 1.57 h^{-1} for 1 and 2 mol% loading of **2**, see Figure S14).

Additionally, we studied whether **1** interacts with HBPin (i.e., forming an active Sn*H* species) or with the polar C=O group of the bezaldehyde. To investigate the potential formation of an Sn*H* moiety, **1** was mixed with 5 equivalents of HBPin in 2 mL of THF-d8. ^{1}H-NMR analysis showed no reaction between **1** and HBPin after 2 h, and no hydridic Sn*H* signal was detected (Figure S22). Similarly, the reaction of **1** and 5 eq. of benzaldehyde in 2 mL of THF-d8 was performed as an NMR-scale experiment. The ^{1}H NMR spectrum displayed the C*H*=O chemical shift of free PhCHO at δ 9.64 ppm as a major component; however, a new strongly deshielded minor signal at δ 10.46 ppm was observed, which was tentatively assigned to a C*H*=O group coordinating to the electrophilic Sn(II) center of **1** (Figure S23). This was further corroborated by the ^{119}Sn {^{1}H} NMR chemical shift, which was upfield shifted from −380[8b] to −510 ppm after the addition of benzaldehyde (see Figure S24), suggesting an increase of the coordination sphere at the Sn center as a result of the aldehyde coordination.

Based on these experiments, we proposed the catalytic cycle depicted in Scheme 2. Coordination of the aldehyde with the electrophilic Sn(II) center in **1**, forming **Int-1** as the first and rate-determining step. Subsequently, the activated C=O bond is attacked by HBPin, and catalyst **1** is regenerated.

Computational studies at the B3PW91/6-311+G(2df,p) level of theory, including THF as a solvent environment, support the suggested mechanism. Initial coordination of benzaldehyde to the Sn-center in **1** forming **Int-1** is an exergonic process by ΔG = −7.3 kJ/mol, whereas the coordination of HBPin to **1** is highly endergonic (Table S1 and Figure S64). As a next possible step, the coordination of HBPin to the intermediate **Int-1** is moderately endergonic by $\Delta\Delta G$ = 24.4 kJ/mol. Finally, regeneration of **1** and formation of the ester are exergonically favored by $\Delta\Delta G$ = −130.0 kJ/mol.

The most active catalyst, **1**, was further examined for a possible carbonyl substrate scope. Thus, several substituted aldehydes (Figures S25–S37) and ketones (Figures S38–S42) were tested in the hydroboration reactions catalyzed by **1** under optimized conditions, as monitored by FTIR spectroscopy (2 mol% of **1**, 0.5 mmol of substrate, 0.5 mmol of HBPin in 2 mL of C_6D_6, and 15 min). The mixtures were stirred at RT, and the conversions of the substrates were verified by ^{1}H NMR spectroscopy after 15 min (Scheme 3).

In general, **1** serves as an active catalyst in the hydroboration of all investigated substrates. Thus, the selected substituted benzaldehydes showed high conversions at these conditions. However, steric shielding (two Me substituents) or polarity change (*p*-substituted NO_2) of the CH=O group lowered the conversion (~70%, Figure 4b,c) compared to the parent benzaldehyde (>95%).

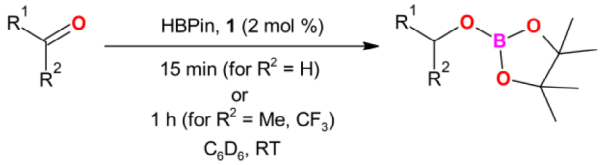

Scheme 3. Hydroboration of substituted carbonyls catalyzed by **1** (2 mol%), 15 min (aldehydes) or 1 h (ketones), RT, C_6D_6.

It should be noted that hydroboration of 4-nitrobenzaldehyde is selective, and the nitro group is not affected during reduction, which is in contrast to 4-hydroxobenzaldehyde (Figure 4d), where two equivalents of HBPin were needed due to the reaction with the OH group (>99%). In the case of 2-bromoisophthalaldehyde, both carbonyl groups were fully reduced (Figure 4e). For aliphatic aldehydes, conversions of up to 83% were detected after 15 min (Figure 4f–g). Interestingly, the hydroboration of various heterocyclic carbaldehydes (Figure 4h–n) was also investigated, with conversions of up to 95%. These results demonstrate the versatility of **1** in the synthesis of a broad range of heterocyclic boronic esters, although the hydroboration of *N*-heterocycles catalyzed by main-group elements remains a largely unexplored area of research.[10] In contrast to the aldehyde, the hydroboration of ketones is more challenging.[4,6] Therefore, we also tested the capability of **1** as a catalyst for the hydroboration of ketones (Figure 4o–s). While the reduction of acetophenone and 2,2,2-trifluoroacetophenone was complete within 1 hour, 2-bromoacetophenone reached 76% conversion, 4-phenyl-3-buten-2-one was reduced to 67%, and benzophenone showed only 20% conversion under identical conditions.

Comparing the catalytic performance of **1** to other Sn-based catalysts, establishing **1** as an efficient catalyst. In particular, complete reduction of benzaldehyde by HBPin was detected within 30 min for the Sn-based catalysts **C** (0.1 mol%), **H** (0.025 mol%), and **I** (0.5 mol%).[5b,6] Other Sn-based catalysts, including **A** (0.05 mol%),[4] **B** (1 mol%),[5a] **E** (0.5 mol%),[5d] and **G** (0.25 mol%),[5f] were also able to fully reduce benzaldehyde, but prolonged reaction times were required, varying from 1 to 2.5 h.[5] Complexes **D** and **F** required higher loadings (1 and 5 mol%) and longer times (4 and 3 h) for the benzaldehyde hydroboration with conversions of 93 and 97%.[5c,e] Metallocene **J** (2.5 mol%, 0.33 h) reduced *p*-substituted benzaldehydes with more than 90% of conversion.[7] Since complex **1** is able to almost completely catalyze the reduction of benzaldehyde by HBPin within 5 min with a 0.01 mol% loading, this Sn-based catalyst is one of the most efficient ones reported to date. In addition, **1** can be applied to a broad substrate scope and shows high tolerance toward various aldehydes and ketones. Thus, complex **1** is highly electrophilic and drives the hydroboration reaction via $R_2C{=}O{\rightarrow}Sn$ interaction.

Interestingly, C_6D_6 solutions of the pyridine-substituted boronic esters showed blue-green photoluminescent (PL) emission under UV-light (365 nm) illumination. In contrast, solutions of other substrates, including furane-, thiophene-, or thiazole-based derivatives, did not show PL under UV irradiation (365 and 395 nm). Therefore, we used **1** as a catalyst for the up-scale hydroboration reaction and prepared new pyridine-substituted boronic esters on a gram scale.

2.2. Synthesis, Characterization, and Photoluminescent Properties of Pyridine-Substituted Boronic Esters

Pyridine-substituted carbaldehydes (Figure 4i–n) were treated with HBPin or 9-BBN in the presence of **1** as the 2 mol% catalyst in C_6H_6 as large-scale experiments.

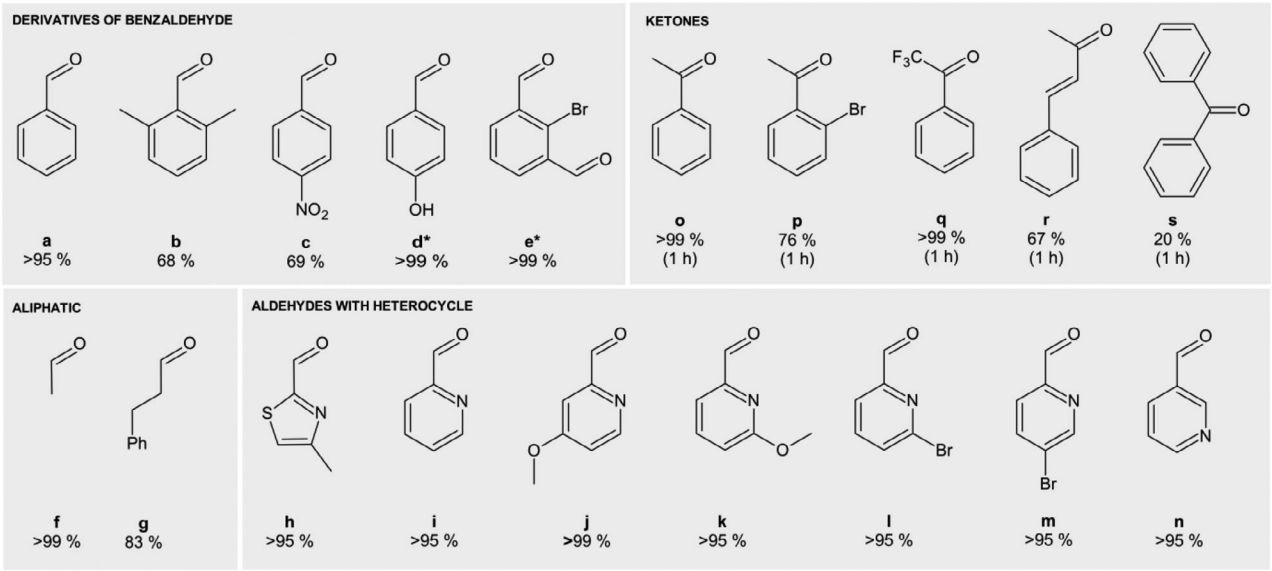

Figure 4. Substrate scope along with achieved conversions (in %) in the hydroboration of carbonyls catalyzed by **1** (2 mol%), 15 min (aldehydes) or 1 h (ketones), RT, C6D6. *2 eq. of HBPin were used due to parallel hydroboration of the OH group d) and the presence of 2 formyls e). Conversions (in %) are detected by ^{1}H NMR.

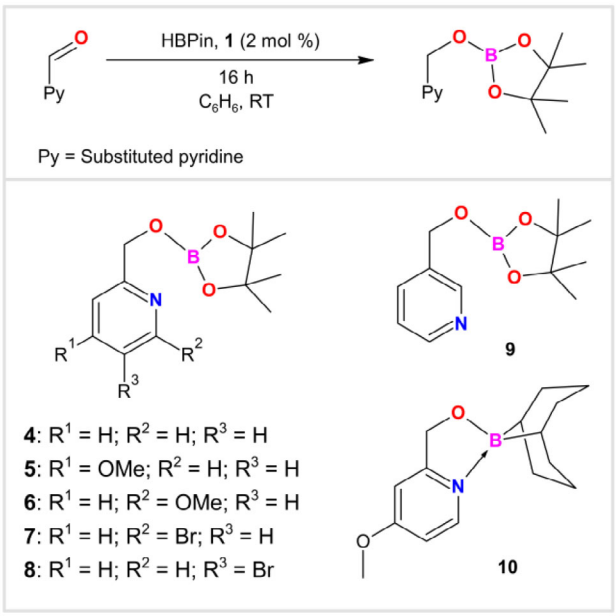

Figure 5. *N*-substituted boron esters **4–10** prepared by up-scale catalyzed hydroboration.

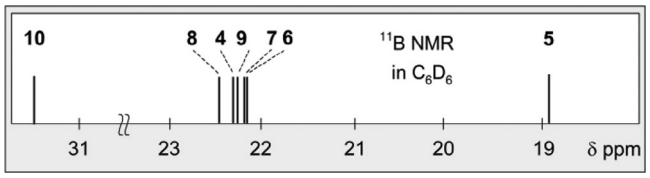

Figure 6. $^{11}B\{^1H\}$ NMR stick diagram for **4–10**. For **4** and **9**, see Ref. [10].

New pyridine-substituted boronic esters [2-(PinBOCH$_2$)-C$_5$H$_4$N] (**4**), [2-(PinBOCH$_2$)-4-(MeO)-C$_5$H$_3$N] (**5**), [2-(PinBOCH$_2$)-6-(MeO)-C$_5$H$_3$N] (**6**), [2-(PinBOCH$_2$)-6-Br-C$_5$H$_3$N] (**7**), [2-(PinBOCH$_2$)-5-Br-C$_5$H$_3$N] (**8**), [3-(PinBOCH$_2$)-C$_5$H$_4$N] (**9**), and borinate [2-[(BBN)OCH$_2$]-4-(MeO)-C$_5$H$_3$N] (**10**) (Figure 5) were isolated after the workup. All new compounds **5–8** and **10** were characterized by NMR spectroscopy (Figures S43–S57) and X-ray structure analysis (for **4**, **5**, and **10**). Finally, their photophysical properties were studied. Compounds **4** and **9** have already been characterized by NMR spectroscopy, and our NMR data match those reported in the literature.[11]

In ^{1}H NMR spectra, signals of the starting C*H*═O protons are missing, while signals of the C*H*$_2$O groups, products of hydroboration, resonate in the narrow range δ 4.71–5.16 ppm. The signals of O*Me* protons resonate at δ 3.71 (**5**), 3.87 (**7**), and 2.99 (**10**) ppm. In the $^{11}B\{^1H\}$ NMR spectra of **4** and **6–9**, the signals appear in the narrow range of δ 22.2–22.5 ppm (Figure 6). These shifts are characteristic of three-coordinated *B*O$_3$ fragments, and the values are very similar to those found for the *N*-unsubstituted (PinB)OCH$_2$C$_6$H$_5$ (δ 22.4 ppm).[12] Therefore, the $^{11}B\{^1H\}$ NMR data exclude the presence of N→B intramolecular coordination in solutions of **4** and **6–9**. The presence of four coordinated boron atoms due to N→B coordination in boron ester is typically associated with upfield shifts of the $^{11}B\{^1H\}$ NMR chemical shifts ranging from δ 4.26 to 13.5 ppm (Figure S58).[13]

To prove the absence of the N→B coordination in solutions of **4** and **6–9**, we treated compound **8** with an excess of the strong *N*-donor DMAP (*p*-dimethylaminopyridine) in C$_6$D$_6$ and measured the $^{11}B\{^1H\}$ NMR spectrum. The $^{11}B\{^1H\}$ NMR revealed two signals at δ 22.7 ppm for **8** and at δ 13.6 ppm, which can be assigned to the DMAP adduct of **8** (see Figure S59). The $^{11}B\{^1H\}$ NMR spectrum of **5** revealed a signal at δ 18.9 ppm, shifted upfield as compared to **4** and **6–9**. This may suggest the presence of a weak N→B interaction in the solution of **5**. Finally, a chemical shift of δ 31.5 ppm was detected in the $^{11}B\{^1H\}$ NMR spectrum of **10**. This value is shifted upfield as compared to the value found for the *N*-unsubstituted (BBN)OCH$_2$C$_6$H$_5$ (δ 57.3 ppm)[12a] but shifted downfield compared to N→B four-coordinated borinates (Figure S58), where the values range from δ 7.8 to 10.8 ppm.[13a,d,14] Again, the $^{11}B\{^1H\}$ NMR spectrum of **10** suggests the existence of a weak N→B interaction in the solution.

The molecular structures of **4**, **5**, and **10** were characterized by X-ray structure analysis (see Table S1) and are depicted in Figure 7 together with the selected bond lengths (Å) and angles (°).

In contrast to the results found in solution, where no or weak N→B interaction was proposed, the solid-state structures of **4**, **5**, and **10** revealed the existence of N→B dative bonds. The B(1)—N(1) bond distances of 1.628(5) Å (**4**), 1.615(1) Å (**5**), and 1.633(3) Å (**10**) are close to the sum of the covalent radii of the parent atoms ($\Sigma_{B,N}$ = 1.56 Å)[15] and are close to the values found in related *N*-coordinated compounds (ranging from 1.6074(19) to 1.633(3) Å for boron esters and from 1.642(1) to 1.655(2) Å for borinates) (Figure S58).[13,14] All compounds contain four coordinated B(1) atoms with a tetrahedral arrangement. Hydroboration of the CH═O also provided new CH$_2$OB fragments with bond distances of C(6)—O(1) (1.411(4) Å (**4**), 1.410(1) Å (**5**), and 1.371(2) Å (**10**)) reaching the length of the covalent single C—O bond (Σ_{C-O} = 1.38 Å).[15]

In general, four coordinated organoboron compounds are promising light-emitting materials.[16–20] These materials usually contain π-conjugated organic molecules that are bridged by four coordinate boron. Therefore, studies involving the molecular design of four coordinated boron compounds are closely linked to potential applications in optoelectronics, including organic light-emitting diodes (OLEDs),[16,17] organic field-effect transistors,[18] photoresponsive materials,[17–19] sensors,[20] and imaging materials.[21] While N-coordinated compounds with the compositions N→BR$_3$, N→B(OR)R$_2$, or N→B(OR)$_2$R (R = alkyl or aryl) were intensively studied for their PL properties,[17] N→B(OR)$_3$ compounds remain relatively unexplored.[13f] Toluene solutions of all *N*-substituted boron esters **4–10** exhibit a weak charge transfer absorption band (ε~50–150 M^{-1} cm^{-1}) with a maximum at 340 to 380 nm in the UV–vis spectra (Figure S60). Excitation wavelength 350 nm was used for all complexes **4–10**. Complexes **4**, **5**, **8**, and **9** exhibited blue-green fluorescence with maximum emission peaks in the narrow range at 469 nm (**4**), 483 nm (**5**), 473 nm (**8**), and 450 nm (**9**) in toluene (Figure 8). On the contrary, compounds **6** and **7** showed no emission under these conditions, indicating the strong effect of the *o*-substitution at the pyridine ring, as both compounds **6** and **7** contain *o*-Br or *o*-OMe substituents. In toluene solutions, compounds **4** and **9** exhibited weak emission, with extremely low

quantum yields (Φ) ranging from 0.006 to 0.009. Compounds **5** and **8** demonstrated enhanced emission efficiencies compared to **4** and **9** but still showed low quantum yields of Φ = 0.03 and 0.04 (see Figure S61).

To evaluate the influence of substituents at the boron center on the photophysical properties, the emission spectrum of **5** was compared with that of the *N*-substituted borinate **10**. Notably, compound **10** exhibited a redshifted emission maximum at 550 nm under identical conditions. However, this spectral shift was accompanied by a markedly reduced quantum yield (Φ = 0.005; see Figure S62), indicating that substitution at the boron atom significantly affects both the emission wavelength and quantum yield.

In the CIE diagram, an area of boron esters **4**–**9** with coordinates in the range *X* = 0.2–0.25; *Y* = 0.24–0.31 and separated borinate **10** with *X* = 0.32; *Y* = 0.4 can be found (Figure 8b). Thus, compound **10** is an interesting luminescent material with a broad emission band in a wide range of the visible spectrum with CIE coordinates close to white light emitters (*X* = 0.33, *Y* = 0.33).[22]

Complex **5**, with the most intensive emission band in solution, was also studied in the solid state. An excitation wavelength of 350 nm was used for the yellow powder of **5** to gain an emission band peaked at 505 nm redshifted from the solution experiment (483 nm). This shift can be attributed to the more stable N→B bond in the rigid solid-state structure. Finally, the quantum yield of the most luminescent active compound, **5**, was determined to be 0.12 in the solid state (Figure S63).

Additional solvent-dependent studies were performed for **5** (see Figure 9), employing an excitation wavelength of 350 nm, consistent with previous measurements in toluene. Emission spectra were recorded in various coordinating (MeCN, THF, water) and weakly coordinating solvents (EtOAc, DCM). In all cases, compound **5** exhibited observable emission bands, indicating that none of the investigated solvents quenched the luminescence. Compared to non-coordinating toluene, the emission maxima in all other solvents were broader and blue-shifted, with the most pronounced spectral changes observed in strongly donating solvents such as THF and MeCN. This also demonstrates the lability of N→B coordination in solution that was also proven experimentally (see Figure S59).

3. Conclusion

N-coordinated Sn(II) cations [{(2,6-*i*Pr$_2$-C$_6$H$_3$)-N=C(Me)-(6-MeO)-C$_5$H$_3$N}SnCl](SnCl$_3$) (**1**), [{(2,6-*i*Pr$_2$-C$_6$H$_3$)-N=C(Me)-(6-P(O)(O*i*Pr)$_2$)-C$_5$H$_3$N}SnCl](SnCl$_3$) (**2**), and [{(1,2-(C$_5$H$_4$N-2-CH=N)$_2$CH$_2$CH$_2$)}SnCl](SnCl$_3$) (**3**) were prepared and used as potential catalysts in the hydroboration reactions of various ketones and aldehydes. It was shown that the efficiency of the catalysts **1**–**3** strongly depends on the coordination number of the tin(II) center, defining a k^2-*N*,*N*-three-coordinated Sn(II) cation in **1** as the most efficient catalyst. Mechanistic and kinetic studies using NMR and IR spectroscopy suggest that the electrophilic species interact with the C=O bond of substrates via an R$_2$C=O→Sn interaction as the rate-determining step, followed by the reaction with HBPin, which is also supported by DFT computations. Time-resolved FTIR spectroscopy showed fast conversion of benzaldehyde during the hydroboration catalyzed by **1** as a pseudo-first-order reaction with $k = 70.2\ h^{-1}$ for 2 mol% of **1**. Investigation of the scope of substrates demonstrated that complex **1** is a highly efficient Sn-based catalyst, suitable for the hydroboration reactions of substituted benzaldehydes, heterocyclic carbaldehydes, and aliphatic aldehydes, as well as ketones. Finally, complex **1** was used for large-scale hydroboration reactions of pyridine-substituted carbaldehydes to prepare

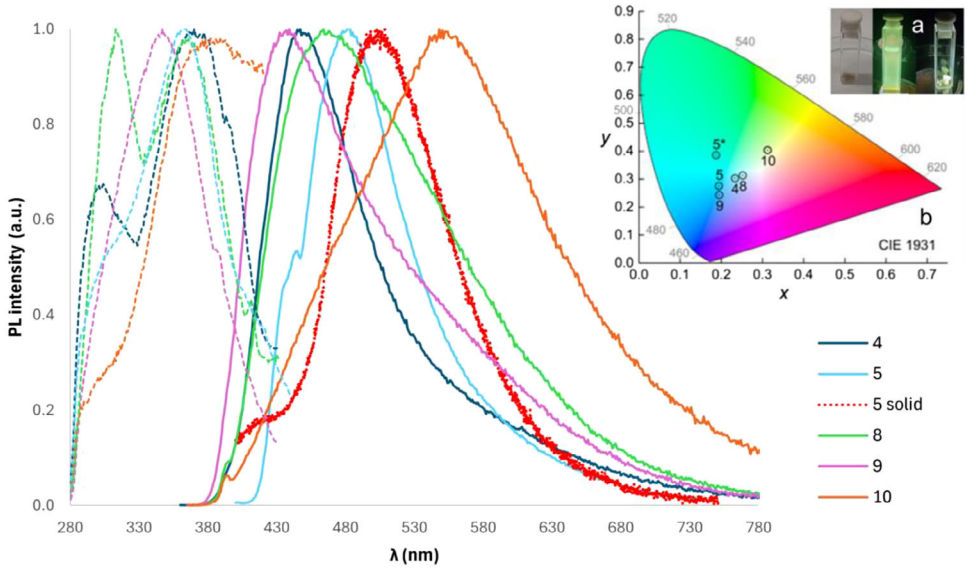

Figure 8. Excitation (dashed) and emission (solid) spectra of photoluminescent compounds **4**, **5**, **8**, **9**, and **10** in toluene solution and emission spectrum of **5** in powder (dotted). a) Compound **5** as a solid (left) and under 365 nm illumination (middle: toluene solution; right: solid). b) CIE chromaticity diagram of the emission bands of the luminescent compounds **4**, **5**, **8**, **9**, and **10** in toluene and **5*** as powder.

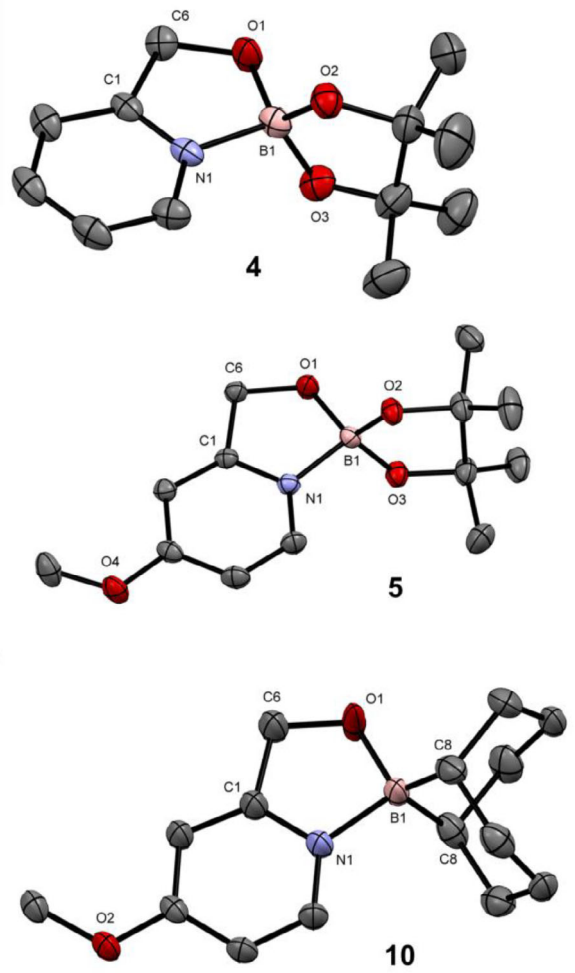

Figure 7. ORTEPs of **4**, **5**, and **10** with 50% probability ellipsoids. H atoms are omitted for clarity. For 4: Bond lengths (Å) and angles (°): B(1)—N(1) 1.628(5), B(1)—O(1) 1.465(4), B(1)—O(2) 1.438(4), B(1)—O(3) 1.434(4), C(6)—O(1) 1.411(4); O(1)—B(1)—N(1) 98.3(3). For **5**: B(1)—N(1) 1.615(1), B(1)—O(1) 1.465(1), B(1)—O(2) 1.443(1), B(1)—O(3) 1.445(2), C(6)—O(1) 1.410(1); O(1)—B(1)—N(1) 98.46(7). For **10**: B(1)—N(1) 1.633(3), B(1)—O(1) 1.492(3), B(1)—C(8) 1.599(3), C(6)—O(1) 1.371(3); O(1)—B(1)—N(1) 97.5.

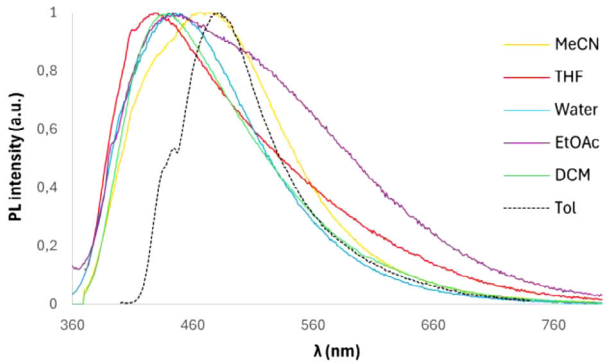

Figure 9. Emission bands of **5**. Solvent-dependent study.

pyridine-substituted boronic esters **4**–**10**, which were characterized using NMR spectroscopy and X-ray structure analysis. Investigation of their photoluminescent properties indicates an important role of N→B coordination for photoluminescent properties. While complex **5** with an N→B interaction provided the most intensive emission band at 483 nm, weak emission bands were observed for **4**, **8**, and **9,** where the absence of N→B coordination was determined in solution. The quantum yield (Φ) of **5** was determined to be 0.12 in the solid state.

The *N*-substituted borinate **10** exhibits a redshifted emission band maximum at 503 nm and is an interesting luminescent material with a broad emission band in the visible spectrum with CIE coordinates close to white light emitters ($X = 0.32$; $Y = 0.4$).

4. Experimental Section

4.1. General Procedures

Solvents were dried by standard methods and distilled prior to use. The deuterated solvents were purchased from GenChem and dried over 4 Å molecular sieves. All moisture- and air-sensitive reactions were carried out under an argon atmosphere by using standard Schlenk techniques. Complexes **1**–**3** were prepared according to literature procedures.[8] Aldehydes, ketones, and HBPin were purchased from Sigma-Aldrich. ^{1}H, $^{13}C\{^{1}H\}$, and $^{11}B\{^{1}H\}$ NMR spectra were recorded on a Bruker Avance 400 and 500 MHz NMR spectrometer at 298 K. The ^{1}H and $^{13}C\{^{1}H\}$ NMR spectra were referenced internally to residual proton-solvent and solvent resonances, respectively, and are reported relative to Me_4Si ($\delta = 0$ ppm). Time-resolved infrared spectra were obtained with an Si-ATR dip probe (Art Photonics) on a Nicolet iS50 FT-IR spectrometer in the range of 600–3500 cm^{-1} (resolution 4 cm^{-1}, sampling interval 3.14 s). The melting or decomposition temperature of compounds was determined on a Stuart MP3 thermometer in a glass capillary. Elemental analyses were performed on a LECO-CHNS-932 analyzer. Photoluminescence was measured on a photoluminescence spectrophotometer FLS1000 (Edinburgh Instruments Ltd.). Excitation source: continuous-wave Xe lamp (450 W) with excitation wavelength at 350 nm. Solutions were in SiO_2 cuvettes (400–740 nm, step 1 nm) in non-deaerated dry toluene at RT. The concentration of compounds **4**–**10** in all samples was ~1.6 mmol/L. Solid sample **5** (300–900 nm, step 0.2 nm) was measured in a $BaSO_4$-coated integrating sphere. Other compounds are liquids, or the solids turn to liquids in the air, so these compounds were not measured in $BaSO_4$-coated integrating sphere. Alternatively, quantum yields of the toluene solutions were recorded using a Quantaurus-QY absolute PL quantum yield spectrometer C11347 by Hamamatsu.

4.2. General Procedure for the Synthesis of *N*-Substituted Boranes

The corresponding pyridine-carbaldehyde was dissolved in 3 mL of C_6H_6 together with 2 mol% of the catalyst **1**. 1.1 eq of HBPin was added by the syringe at the RT. The reaction mixture was stirred for 16 h at RT. Then the volatiles were evaporated under reduced pressure. Solid products **4**, **5**, and **10** were washed by a small amount of hexane and dried.

*Characterization of [2-(PinBOCH$_2$)-4-(MeO)-C$_5$H$_3$N] (**5**)*: Yellow powder. Yield: 97%. Mp: 95–96 °C. Anal. Calcd for $C_{13}H_{20}BNO_4$ ($M_w = 265.11$) C, 58.9; H, 7.6. Found: C, 59.1; H, 7.6. ^{1}H NMR (C_6D_6, 400.13 MHz): δ (ppm) 1.18 (s, 12H, CH_3-Pin), 2.99 (s, 3H, CH_3O), 5.13 (s,

2H, CH_2), 6.21 (d, 1H, Ar-C^5H, $^3J(^1H, ^1H)$ = 5.9 Hz), 6.65 (s, 1H, Ar-C^3H), 8.22 (d, 1H, Ar-C^6H, $^3J(^1H, ^1H)$ = 5.8 Hz). $^{13}C\{^1H\}$ NMR (C_6D_6, 100.613): δ (ppm) 19.8 (CH_3-Pin), 49.3 (CH_3O), 61.8 (C-Pin), 76.4 (CH_2), 99.4; 104.2 (Ar-$C^{3,5}$), 142.2; 156.6; 161.8 (Ar-$C^{2,4,6}$). $^{11}B\{^1H\}$ NMR (C_6D_6, 128.378): δ (ppm) 18.9.

*Characterization of [2-(PinBOCH$_2$)-6-(MeO)-C$_5$H$_3$N] (**6**)*: Colorless oil. Yield: 98%. Anal. Calcd for $C_{13}H_{20}BNO_4$ (M_w = 265.11) C, 58.9; H, 7.6. Found: C, 58.7; H, 7.5. ^1H NMR (C_6D_6, 400.13 MHz): δ (ppm) 1.04 (s, 12H, CH_3-Pin), 3.71 (s, 3H, CH_3O), 5.06 (s, 2H, CH_2), 6.47 (d, 1H, Ar-C^3H, $^3J(^1H, ^1H)$ = 8.3 Hz), 6.98 (d, 1H, Ar-C^5H, $^3J(^1H, ^1H)$ = 7.3 Hz), 7.15 (m, 1H, Ar-C^4H). $^{13}C\{^1H\}$ NMR (C_6D_6, 125.613): δ (ppm) 24.3 (CH_3-Pin), 52.6 (CH_3O) 67.3 (C-Pin), 82.5 (CH_2), 109.2; 112.1 (Ar-$C^{3,5}$), 138.8 (Ar-C^4); 157.2; 163.6 (Ar-$C^{2,6}$). $^{11}B\{^1H\}$ NMR (C_6D_6, 160.462): δ (ppm) 22.2.

*Characterization of [2-(PinBOCH$_2$)-6-Br-C$_5$H$_3$N] (**7**)*: Light yellow oil. Yield: 97%. Anal. Calcd for $C_{12}H_{17}BBrNO_3$ (M_w = 313.98) C, 45.9; H, 5.5. Found: C, 46.1; H, 5.4. ^1H NMR (C_6D_6, 500.13 MHz): δ (ppm) 1.03 (s, 12H, CH_3-Pin), 4.99 (s, 2H, CH_2), 6,72 (t, 1H, Ar-C^4H, $^3J(^1H, ^1H)$ = 7.7 Hz), 6.85 (d, 1H, Ar-C^3H, $^3J(^1H, ^1H)$ = 7.7 Hz), 7.07 (d, 1H, Ar-C^5H, $^3J(^1H, ^1H)$ = 7.7 Hz). $^{13}C\{^1H\}$ NMR (C_6D_6, 125.613): δ (ppm) 24.5 (CH_3-Pin), 66.8 (C-Pin), 82.9 (CH_2), 118.5; 126.2; 138.6 (Ar-C^{3-5}), 141.4; 160.9 (Ar-$C^{2,6}$). $^{11}B\{^1H\}$ NMR (C_6D_6, 128.378): δ (ppm) 22.3.

*Characterization of [2-(PinBOCH$_2$)-5-Br-C$_5$H$_3$N] (**8**)*: Light yellow oil. Yield: 97%. Anal. Calcd for $C_{12}H_{17}BBrNO_3$ (M_w = 313.98) C, 45.9; H, 5.5. Found: C, 46.1; H, 5.6. ^1H NMR (C_6D_6, 400.13 MHz): δ (ppm) 1.03 (s, 12H, CH_3-Pin), 5.06 (s, 2H, CH_2), 7.02 (d, 1H, Ar-C^3H, $^3J(^1H, ^1H)$ = 8.3 Hz), 7.17 (m, 1H, Ar-C^4H), 8.47 (s, 1H, Ar-C^6H). $^{13}C\{^1H\}$ NMR (C_6D_6, 100.613): δ (ppm) 19.2 (CH_3-Pin), 61.8 (C-Pin), 77.5 (CH_2), 113.5; 116.0 (Ar-$C^{3,5}$), 133.5; 144.6; 152.8 (Ar-$C^{2,4,6}$). $^{11}B\{^1H\}$ NMR (C_6D_6, 128.378): δ (ppm) 22.5.

*Characterization of [2-[(BBN)OCH$_2$]-4-(MeO)-C$_5$H$_3$N] (**10**)*: Light-brown powder. Yield: 95%. Mp: 216–218 °C. Anal. Calcd for $C_{15}H_{22}BNO_2$ (M_w = 259.15) C, 69.5; H, 8.6. Found: C, 69.9; H, 8.8. ^1H NMR ($CDCl_3$, 500.13 MHz): δ (ppm) 0.58 (bs, 2H, B-CH), 1.52 (bs, 2H, BBN), 1.68 (bs, 4H, BBN), 1.86 (bs, 6H, BBN), 3.87 (s, 3H, CH_3O), 4.99 (s, 2H, CH_2), 6.80 (s, 2H, Ar-C^{3+5}H), 8.48 (d, 1H, Ar-C^6H, $^3J(^1H, ^1H)$ = 6.5 Hz). $^{13}C\{^1H\}$ NMR ($CDCl_3$, 125.613): δ (ppm) 24.4 (B-C), 32.1 (BBN), 56.1 (CH_3O), 67.0 (CH_2), 104.1; 109.6; 143.2 (Ar-$C^{3,5,6}$), 162.3; 167.9 (Ar-$C^{2,4}$). $^{11}B\{^1H\}$ NMR ($CDCl_3$, 128.378): δ (ppm) 31.5.

4.3. Catalytic Study: Typical Procedure for Hydroboration of Aldehydes and Ketones Catalyzed by 1–3

Complex **1** (0.01 mmol; 2 mol%) was dissolved in 2 mL of C_6D_6 solution of corresponding aldehyde or keton (0.5 mmol) in a Schlenk tube under an inert atmosphere of argon, and 1 eq. of HBPin (0.5 mmol) was added by syringe. The mixture was stirred at RT, and the reaction was monitored by ^1H NMR after 15 min for aldehydes or after 60 min for ketones.

4.4. FTIR Kinetic Study

The IR probe was placed into the Schlenk tube with benzene (5 mL) solution of catalyst **1** (0, 1, or 2 mol%) with benzaldehyde (0.5 mmol), and 0.5 mol of HBPin was added at once via syrinx. Time-dependent changes of band height at 1705 (baseline 1735−1680 cm^{-1}), 1341 (1403–1277), and 967 cm^{-1} (930–981) were monitored. From the obtained data, the conversion of both benzaldehyde and HBPin was calculated together with the formation of the product (boronic ester) for systems catalyzed with 1 and 2 mol% of **1**; see Figures S10–S12.

4.5. Crystallography

Single crystals of **4** were grown from hexane at 5 °C. Single crystals of **5** were grown from hot saturated Et_2O. Single crystals of **10** were received from toluene by slow evaporation at room temperature. Full sets of diffraction data for **4**, **5**, and **10** were collected at 150(2)K with a Bruker D8-Venture diffractometer equipped with Cu (Cu/Kα radiation; λ = 1.54178 Å) or Mo (Mo/Kα radiation; λ = 0.71073 Å) microfocus X-ray (IμS) sources. A Photon CMOS detector and an Oxford Cryosystems cooling device was used for data collection. The frames were integrated with the Bruker SAINT software package using a narrow-frame algorithm. Data were corrected for absorption effects using the Multi-Scan method (SADABS). Obtained data were treated by XT-version 2018/1 and SHELXL-2017/1 software implemented in APEX3 v2016.5-0 (Bruker AXS) system.[23] Hydrogen atoms were mostly localized on a difference Fourier map; however. to ensure uniformity of treatment of crystal, all hydrogen atoms were recalculated into idealized positions (riding model) and assigned temperature factors, $H_{iso}(H)$ = 1.2 Ueq (pivot atom) or of 1.5 Ueq (methyl). H atoms in methyl, methylene, and methine and hydrogen atoms in aromatic rings were placed with C−H distances of 0.99, 0.98, 0.97, and 0.95 Å, respectively, and 0.82 Å for OH.[24]

Acknowledgments

The work was supported from ERDF "'Innovative materials suitable for high added value applications (INMA)'" (No. CZ.02.01.01/00/23_021/0008593).

Open access publishing facilitated by Univerzita Pardubice, as part of the Wiley - CzechELib agreement.

Conflict of Interests

The authors declare no conflict of interests.

Data Availability Statement

The Supporting Information is available free of charge. NMR and IR spectra, crystallographic parameters, catalytic and mechanistic studies, absorption spectra of **4**–**10** in toluene.

Keywords: Cationic complex · Hydroboration · Photoluminescence · Tin

[1] a) H. C. Brown, *Hydroboration*, W. A. Benjamin, New York, USA **1962**. b) A. Pelter, K. Smith, H. C. Brown, *Borane Reagents*, Academic Press, London **1988**.
[2] a) A. Y. Khalimon, P. Farha, L. G. Kuzminab, G. I. Nikonov, *Chem. Commun.* **2012**, *48*, 455–457. b) M. J. Sgro, D. W. Stephan, *Angew. Chem. Int. Ed.* **2012**, *51*, 11343–11345. c) D. Männig, H. Nöth, *Angew. Chem. Int. Ed.* **1985**, *24*, 878–879.
[3] a) M. L. Shegavi, S. K. Bose, *Catal. Sci. Technol.* **2019**, *9*, 3307–3336 b) N. Sen, S. Khan, *Chem Asian J.* **2021**, *16*, 705–719.
[4] T. J. Hadlington, M. Hermann, G. Frenking, C. Jones, *J. Am. Chem. Soc.* **2014**, *136*, 3028–3031.
[5] a) Y. Liu, X. Liu, Y. Liu, W. Li, Y. Ding, M. Zhong, X. Ma, Z. Yang, *Inorg. Chim. Acta* **2018**, *471*, 244-248. b) V. Nesterov, R. Baierl, F. Hanusch, A. E. Ferao, S. Inoue, *J. Am. Chem. Soc.* **2019**, *141*, 14576–14580. c) R. Dasgupta, S. Das, S. Hiwase, S. K. Pati, S. Khan, *Organometallics* **2019**, *38*, 1429–1435.

d) K. Nakaya, S. Takahashi, A. Ishii, K. Boonpalit, P. Surawatanawong, N. Nakata, *Dalton Trans.* **2021**, *50*, 14810–14819. e) S. Pahar, V. Sharma, S. Tothadi, S. S. Sen, *Dalton Trans.* **2021**, *50*, 16678–16684. f) K. V. Arsenyeva, A. V. Klimashevskaya, K. I. Pashanova, O. Y. Trofimova, M. G. Chegerev, A. A. Starikova, A. V. Cherkasov, G. K. Fukin, I. A. Yakushev, A. V. Piskunov, *Appl. Organomet. Chem.* **2022**, *36*, e6593.

[6] a) M. K. Sharma, M. Ansari, P. Mahawar, G. Rajaraman, S. Nagendran, *Dalton Trans.* **2019**, *48*, 664–672. b) X. X. Zhao, J. A. Kelly, A. Kostenko, S. Fujimori, S. Inoue, *Z. Anorg. Allg. Chem.* **2022**, *648*, e202200220.

[7] H. J. Robertson, M. N. Fujiwara, A. L. Liberman-Martin, *Polyhedron* **2024**, *250*, 116837.

[8] a) M. Novák, J. Turek, Y. Milasheuskaya, Z. Růžičková, Š. Podzimek. R. Jambor, *Dalton Trans.* **2021**, *50*, 16039–16052. b) M. Bouška, L. Dostál, A. Růžička, R. Jambor, *Organometallics* **2013**, *32*, 1995–1999.

[9] a) G. Socrates, *Infrared and Raman Characteristic Group Frequencies: Tables and Charts*, John Wiley & Wiley, Chichester, UK **2001**, pp. 143–149. b) T. Ghatak, K. Makarov, N. Fridmana, M. S. Eisen, *Chem. Commun.* **2018**, *54*, 11001–11004. c) H. Stachowiak, J. Kaźmierczak, K. Kuciński, G. Hreczycho, *Green Chem.* **2018**, *20*, 1738–1742.

[10] a) J. R. Lawson, L. C. Wilkins, R. L. Melen, *Chem. –Eur. J.* **2017**, *23*, 10997–11000. b) R. Kumar, P. Rawal, I. Banerjee, H. Pada Nayek, P. Gupta, T. K. Panda, *Chem. Asian J.* **2022**, *17*, e202200013. c) Z. Zhu, X. Wu, X. Xu, Z. Wu, M. Xue, Y. Yao, Q. Shen, X. Bao, *J. Org. Chem.* **2018**, *83*, 10677–10683. d) O. Moždiak, Z. Růžičková, M. Erben, L. Dostál, R. Jambor, *Eur. J. Inorg. Chem.* **2024**, *27*, e202400193.

[11] a) Z. Huang, D. Liu, J. Camacho-Bunquin, G. Zhang, D. Yang, J. M. López-Encarnación, Y. Xu, M. S. Ferrandon, J. Niklas, O. G. Poluektov, J. Jellinek, A. Lei, E. E. Bunel, M. Delferro, *Organometallics* **2017**, *36*, 3921–3930. b) S. Ataie, S. L. Dudra, E. R. Johnson, R. T. Baker, *ACS Catal.* **2023**, *13*, 10076–10084. c) X. Liu, B. Li, X. Hua, D. Cui, *Org. Lett.* **2020**, *22*, 4960–4965. d) W. Wang, K. Lu, Y. Qin, W. Yao, D. Yuan, S. A. Pullarkat, L. Xu, M. Ma, *Tetrahedron* **2020**, *76*, 131145.

[12] a) Y. Wu, C. Shan, J. Ying, J. Su, J. Zhu, L. L. Liu, Y. Zhao, *Green Chem.* **2017**, *19*, 4169–4175. b) C. C. Chong, H. Hirao, R. Kinjo, *Angew. Chem. Int. Ed.* **2015**, *54*, 190–194.

[13] For N-coordinated boron esters: a) N. Farfán, D. Castillo, P. Joseph-Nathan, R. Contreras, L. Szentpály, *J. Chem. Soc. Perkin Trans. 2* **1992**, *4*, 527–532. b) Pingrong Wei and David A. Atwood, *Inorg. Chem.* **1998**, *37*, 4934–4938. c) J. Huskens, R. Goddard, M. T. Reetz, *J. Am. Chem. Soc.* **1998**, *120*, 6617–6618. d) S. S. Barnes, C. M. Vogels, A. Decken, S. A. Westcott, *Dalton Trans.* **2011**, *40*, 4707. e) V. Stepanenko, M. de Jesús, C. Garcia, C. L. Barnes, M. Ortiz-Marciales, *Tetrahedron Lett.* **2012**, *53*, 910–913. f) W. Duan, K. Li, H. Ji, Y. Huo, Q. Yao, H. Liu, S. Gong, *Dyes Pigm.* **2021**, *193*, 109538.

[14] For N-coordinated borinates: a) S. J. Rettig, J. Trotter, *Can. J. Chem.* **1976**, *54*, 3130–3141. b) J. V. B. Kanth, H. C. Brown, *Tetrahedron* **2002**, *58*, 1069–1074.

[15] P. Pyykkö, M. Atsumi, *Chem. -Eur. J.* **2009**, *15*, 186–197.

[16] a) S. Wang, *Coord. Chem. Rev.* **2001**, *215*, 79-98. b) L. S. Huang, C. H. Chen, *Mater. Sci. Eng. R* **2002**, *39*, 143–222.

[17] a) D. Li, H. Zhang, Y. Wang, *Chem. Soc. Rev.* **2013**, *42*, 8416. b) Y. L. Rao, S. Wang, *Inorg. Chem.* **2011**, *50*, 12263–12274.

[18] Y. Sun, D. Rohde, Y. Liu, L. Wan, Y. Wang, W. Wu, C. Di, G. Yu, D. Zhu, *J. Mater. Chem.* **2006**, *16*, 4499–4503.

[19] a) J. S. Lu, S. B. Ko, N. R. Walters, Y. Kang, F. Sauriol, S. Wang, *Angew. Chem. Int. Ed.* **2013**, *52*, 4544–4548. b) Y. Rao, H. Amarne, J. Lu, S. Wang, *Dalton Trans.* **2013**, *42*, 638–644. c) C. Baik, S. K. Murphy, S. Wang, *Angew. Chem. Int. Ed.*, **2010**, *49*, 8224–8227.

[20] a) T. Agou, M. Sekine, J. Kobayashi, T. Kawashima, *Chem. Commun.* **2009**, *14*, 1894. b) M. Lepeltier, O. Lukoyanova, A. Jacobson, S. Jeeva, D. F. Perepichka, *Chem. Commun.* **2010**, *46*, 7007. c) H. Maeda, Y. Bando, K. Shimomura, I. Yamada, M. Naito, K. Nobusawa, H. Tsumatori, T. Kawai, *J. Am. Chem. Soc.* **2011**, *133*, 9266–9269.

[21] G. M. Fischer, C. Jüngst, M. Isomäki-Krondahl, D. Gauss, H. M. Möller, E. Daltrozzo, A. Zumbusch, *Chem. Commun.* **2010**, *46*, 5289.

[22] a) B. Liu, Z. Chen, B. Chu, Y. L. Wang, N. Li, H. Zhang, Y. Yang, S. Hu, X. H. Zhang, *Adv. Photonics Res.* **2021**, *2*, 2000161.

[23] G. M. Sheldrick, *Acta Crystalllogr.* **2015**, Sect. A, *A71*, 3–8.

[24] Deposition Number(s) 2390463 (for **4**), 2390464 (for **5**) and 2390465 (for **10**) contain(s) the supplementary crystallographic data for this paper. These data are provided free of charge by the joint Cambridge Crystallographic Data Centre and Fachinformationszentrum Karlsruhe Access Structures service (http://www.ccdc.cam.ac.uk/structures).

Manuscript received: March 13, 2025
Revised manuscript received: June 18, 2025
Accepted manuscript online: July 4, 2025
Version of record online: ■■, ■■